

A Comparative Study of Mode Arrivals at Megameter Ranges for 28 Hz, 75 Hz, and 84 Hz Sources

**Kathleen E. Wage, Arthur B. Baggeroer, Theodore G. Birdsall,
Matthew A. Dzieciuch, Bruce M. Howe, James A. Mercer,
Kurt Metzger, Walter H. Munk, Robert C. Spindel, and
Peter F. Worcester**

September 2003

Proceedings of the 2003 IEEE/MTS Oceans Conference, pp. 258-265.

© 2003 IEEE. Personal use of this material is permitted. However, permission to reprint/republish this material for advertising or promotional purposes or for creating new collective works for resale or redistribution to servers or lists, or to reuse any copyrighted component of this work in other works must be obtained from the IEEE.

A Comparative Study of Mode Arrivals at Megameter Ranges for 28 Hz, 75 Hz, and 84 Hz Sources

Kathleen E. Wage,^a Arthur B. Baggeroer,^b Theodore G. Birdsall,^c Matthew A. Dzieciuch,^d
Bruce M. Howe,^e James A. Mercer,^e Kurt Metzger,^c Walter H. Munk,^d Robert C. Spindel,^e
and Peter F. Worcester^d

^aCorresponding author: Electrical & Computer Engineering Department, George Mason University, Fairfax, VA 22030, kwage@gmu.edu

^bMassachusetts Institute of Technology, Cambridge, MA 02139

^cUniversity of Michigan, Ann Arbor, MI 48109

^dScripps Institution of Oceanography, La Jolla, CA 92093

^eApplied Physics Laboratory, University of Washington, Seattle, WA 98195

Abstract—At long range, the low order acoustic modes constitute some of the most energetic arrivals. Prior to using these signals in tomographic or matched field inversions, it is important to understand their fluctuation statistics. Long vertical line arrays installed as a part of the Acoustic Thermometry of Ocean Climate (ATOC) experiment provided a unique opportunity to measure low-order acoustic mode signals at megameter ranges from a broadband source. The ATOC VLA's at Hawaii and Kiritimati received M-sequences transmitted from two sources: a bottom-mounted source on Pioneer Seamount and a near-axial source deployed nearby as a part of the Alternate Source Test (AST). The Pioneer source had a center frequency of 75 Hz, and the AST source had center frequencies of 28 Hz and 84 Hz. Ranges from the sources to the arrays at Hawaii and Kiritimati are on the order of 3.5 and 5.1 megameters, respectively. This paper compares the mode 1 arrivals at the two ranges and three center frequencies. Differences between the arrivals for the bottom-mounted and mid-watercolumn sources are investigated using broadband PE simulations. Temporal coherence of the mode 1 signals is discussed.

I. INTRODUCTION

At long range, the low order acoustic modes constitute some of the most energetic arrivals. The low modes are concentrated around the sound channel axis and have potential applications in tomographic inversions [1]. One of the difficulties in using the low mode signals in tomography or other applications is that the propagation over long ranges is dominated by scattering due to internal waves. The non-adiabatic nature of the propagation makes it difficult to interpret the mode arrival patterns at megameter ranges. Both theoretical [2], [3] and empirical [4], [5] studies have revealed interesting characteristics of the low mode arrivals, but at present there is no adequate theory to describe these signals. A better understanding of how the modes fluctuate in the presence of internal waves is needed if these signals are to be useful in tomography and matched field processing.

Kathleen Wage acknowledges the support an Office of Naval Research Ocean Acoustics Young Faculty Award. Additionally, this research was supported by the Office of Naval Research (Grant N00014-95-1-0800 to APL-UW and Grant N00014-95-1-0589 to SIO) and by the Strategic Environmental Research and Development Program through Defense Advanced Research Project Agency Grant MDA972-93-1-0003. The two HLF-6A low-frequency acoustic sources used in these experiments were modified for operation at depths of up to 1300 m and a specialized handling system was developed for them as part of the Joint Environmental Test Initiative sponsored by SPAWAR PMW-182.

The Acoustic Thermometry of Ocean Climate (ATOC) experiment and the associated Alternate Source Test (AST) provided a unique opportunity to observe broadband low-order mode signals at long ranges. Two vertical line arrays (VLA's) installed for ATOC received M-sequences transmitted from two near-axial sources: one mounted on a seamount and the other suspended from a ship in nearby deeper water. The bottom-mounted source transmitted at a center frequency of 75 Hz and the ship-deployed source transmitted at both 28 Hz and 84 Hz. Ranges from the sources to the two arrays were on the order of 3.5 and 5.1 megameters, as shown in Figure 1. In previous work [6], Wage *et al.* analyzed the 75 Hz receptions at one of the arrays and compiled mode statistics from 5 months of data. The purpose of the present paper is to compare the mode arrivals at different ranges and frequencies and to investigate the differences between receptions from the bottom-mounted source and mid-watercolumn source.

The outline of the paper is as follows. Section II describes the relevant details of the experiments and shows examples of receptions at each range and carrier frequency. In addition this section explores the effects of bathymetry near the source on long-range propagation by comparing the ATOC and AST receptions to broadband simulations. After briefly reviewing the short-Fourier mode processing technique, Section III shows examples of the mode 1 estimates obtained from the experimental data. Section IV examines the temporal coherence of mode 1 using the ATOC and AST experimental data and simulation results. Section V concludes the paper.

II. EXPERIMENT

Figure 1 shows the geodesic paths to the vertical arrays used in the ATOC and AST experiments. Two 40-element VLA's, moored near Hawaii and Kiritimati, received the signals transmitted by the sources located off the California coast. The source-receiver ranges are 3.5 megameters for the Hawaii path and 5.1 megameters for the Kiritimati path. The VLA's were deployed in November 1995 and recovered in August 1996. See [7] for a thorough overview of the ATOC receiver hardware. The following sections review the relevant details of the ATOC and AST transmissions and describe the receptions used in this analysis.

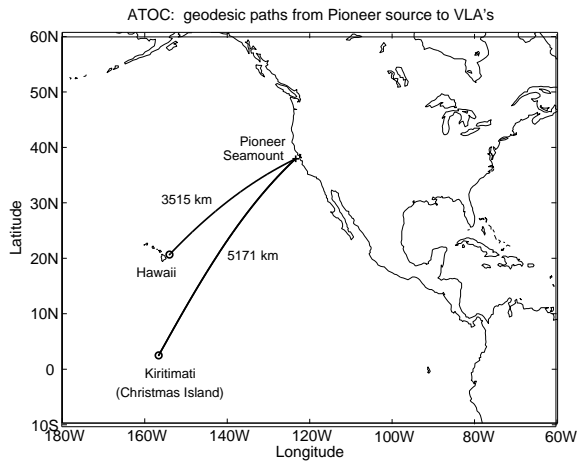


Fig. 1. Geodesic paths from the Pioneer seamount source to the ATOC vertical line arrays at Hawaii and Kiritimati.

A. Transmissions

The ATOC source was located on Pioneer Seamount (indicated in Figure 1) at a depth of approximately 939 m. This source transmitted phase-encoded pseudo-random sequences at a center frequency of 75 Hz. Each transmission consisted of 44 repetitions of the 27.28 second M-sequence. The ATOC Marine Mammal Research Program determined the transmission schedule. During specified periods, the source transmitted for 20 minutes every 4 hours.

Transmissions from Pioneer Seamount were temporarily discontinued during the AST, which took place in late June and early July of 1996. A ship-suspended source was deployed to a depth of 652 m at a position 7 nm southwest of the ATOC Pioneer source. This mid-watercolumn source transmitted pseudo-random sequences at two frequencies simultaneously: 28 Hz and 84 Hz. Each M-sequence was 27.28 seconds long. Most transmissions were for 20 minutes, occurring at intervals of 4 hours, but there were five longer (40 minute) transmissions over the course of the experiment.

B. Receptions

The ATOC VLA's at Hawaii and Kiritimati each consisted of 40 hydrophones with 35 m spacing. For each transmission the VLA's computed four-period averages of the pseudo-random sequence broadcast by the source. The VLA's recorded 10 of these four-period averages (spanning 18.2 minutes) for each regular transmission and recorded 20 four-period averages for the long transmissions from the AST source. After the arrays were recovered, the time series for each of the four-period averages was complex-demodulated and matched-filtered (for pulse compression).

The position of the VLA's was tracked using a long-baseline acoustic navigation system. Navigation data were recorded immediately before and after each transmission. The mooring motion for each sensor was derived from these measurements. Pre-processing for all the receptions discussed in this paper consists of demodulation and matched-filtering, followed by application of the mooring corrections.

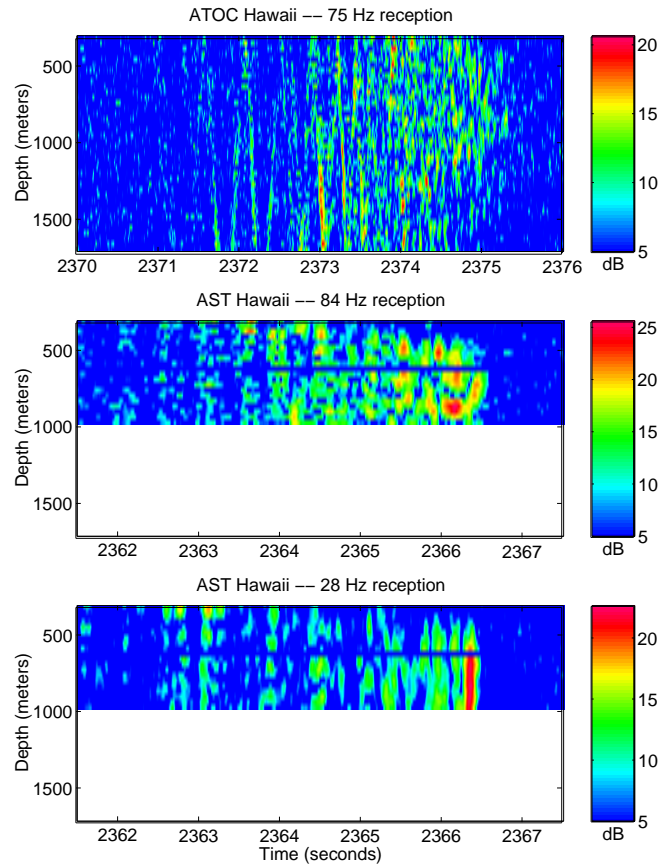


Fig. 2. Receptions at the Hawaii array during the ATOC and AST experiments. The top plot shows a reception of a 75 Hz ATOC source transmission. The bottom two plots are examples of AST receptions at the 84 Hz and 28 Hz center frequencies. The bottom half of the Hawaii array failed prior to the AST experiment, thus the AST signals were received by only the top 20 hydrophones. The 10th hydrophone from the surface also appears to be bad. Note that the top plot has a different starting time than the bottom two plots; the timewidth of all three plots is 6 seconds.

Figure 2 shows representative examples of receptions at the Hawaii array during the ATOC and AST experiments. The top plot shows the received pressure field as a function of time and depth for one of the four-period averages of an ATOC 75 Hz source transmission. The bottom two plots show examples of four-period averages for the 84 Hz and 28 Hz signals from the AST source at the same array. Since the bottom half of the Hawaii VLA failed after approximately 5 months, the AST transmissions were recorded only on the top 20 hydrophones of this array. Note that the starting time for the ATOC reception plot is different from that of the AST plots, due to the fact that the path to Hawaii from the ATOC source is slightly longer than for the AST source. All three of the plots in Figure 2 display a 6 second time interval.

In deep water the high modes travel faster than the low modes. The familiar "accordion" pattern visible in the early part (2371.5 to 2373 seconds) of the 75 Hz reception shown in Figure 2 is due to the constructive interference of the higher order modes. The diffuse finale region (2373.5 to 2375.5 seconds) consists of the lower order mode arrivals. The AST

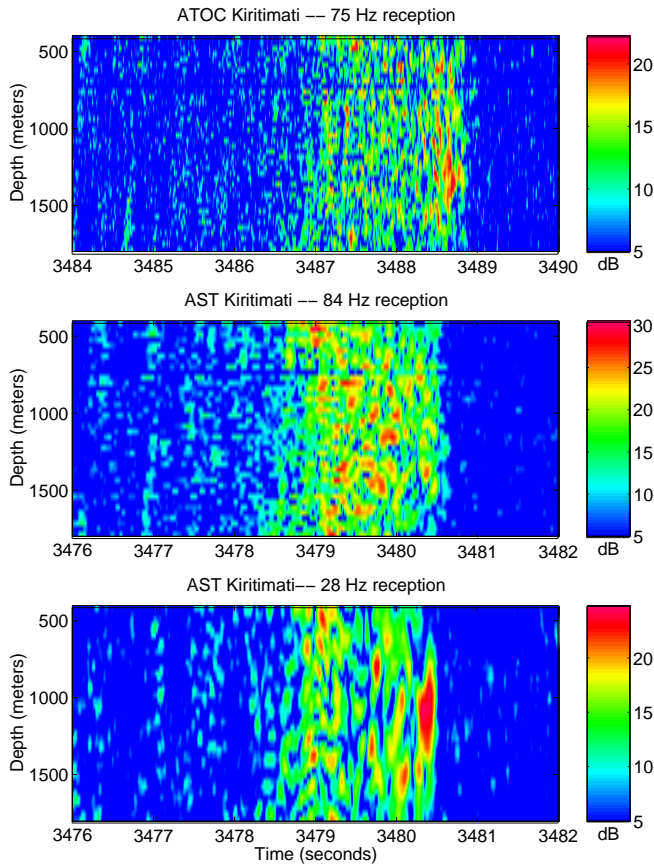


Fig. 3. Receptions at the Kiritimati array during the ATOC and AST experiments. The top plot shows a reception of a 75 Hz ATOC source transmission. The bottom two plots are examples of AST receptions at Kiritimati for the 84 Hz and 28 Hz center frequencies. Note that the top plot has a different starting time than the bottom two plots; the timewidth of all three plots is 6 seconds.

source has a narrower bandwidth than the ATOC source,¹ which is evident in a comparison of the ATOC and AST receptions in Figure 2. Comparing the three plots also reveals that the AST receptions have a sharper final cutoff, which appears to be tapered in depth, *i.e.*, the shallower hydrophones have earlier cutoffs than the deeper hydrophones. The 28 Hz AST reception is dominated by a strong arrival with spatial characteristics similar to mode 1, whereas the finale regions of the 75 Hz and 84 Hz receptions are characterized by much more complicated interference patterns.

Figure 3 shows representative examples of receptions at the Kiritimati array during the ATOC and AST experiments. Unlike at the Hawaii array, the 75 Hz reception at Kiritimati is very similar to the 84 Hz reception. Both the 75 Hz data and the 84 Hz data show a sudden cutoff, with little tapering in depth, *i.e.*, the shallow and deep sensors cut off almost simultaneously. Similar to Hawaii, the 28 Hz reception shown in Figure 3 has a strong arrival with spatial characteristics similar to mode 1.

¹The demodulation filter used in the ATOC processing has a 40 Hz bandwidth, whereas the filter used in the AST processing has a 12 Hz bandwidth.

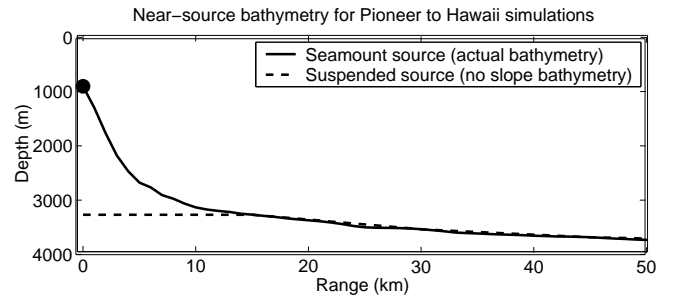


Fig. 4. Bathymetry for the PE simulations. The solid line is the measured bathymetry along the track from Pioneer seamount to the Hawaii VLA. The dashed line is the bathymetry used in the suspended source simulations (the seamount is removed). A large dot indicates the source location.

C. Simulation Comparison: Near-Source Bathymetric Effects

As noted above, the AST receptions at Hawaii exhibit a much sharper cutoff as compared to the ATOC 75 Hz receptions. The purpose of this section is to explore whether bathymetric interactions near the source can account for this difference. The ATOC source is located at a depth of 939.5 meters on Pioneer seamount. Figure 4 shows the actual bathymetry along the path from Pioneer to the Hawaii VLA. At its steepest, the slope of the Pioneer-Hawaii path is approximately 20 degrees.

To examine the effects of the source bathymetry on long-range propagation, consider two broadband simulations implemented using the RAM parabolic equation code [8]. The first simulation places the source on the seamount, using the sloping bathymetry shown in Figure 4. The second simulation keeps the source at the same depth, but removes the seamount, *i.e.*, the bathymetry is as shown by the dashed line in Figure 4. In both simulations the background soundspeed is determined from temperature and salinity profiles for winter, derived from the World Ocean Atlas [9], [10]. The background environment in both cases is perturbed by internal wave fluctuations at $\frac{1}{2}$ Garrett-Munk strength, generated using the method of Colosi and Brown [11]. The center frequency for these simulations is 75 Hz.

Figure 5 shows the results for the simulation that uses the actual bathymetry near the seamount. The top plot in the figure is the synthesized pressure time series at Hawaii. Note that the finale region is not clearly defined by a sharp cutoff, similar to the ATOC reception discussed above. The bottom plot in Figure 5 is the modal time series obtained by projecting the field (finely sampled in depth) onto the mode functions at the receiver. This plot indicates that modes 1-5 have strong arrivals around 2375 seconds, followed by almost a second of weaker arrivals. Figure 6 shows the results of the simulation with the seamount removed. In contrast with the previous simulation, the time series for the suspended source exhibits a very sharp cutoff. Modes 1-5 again have strong arrivals around 2375 seconds, but they are not followed by any weaker arrivals. Note that the finale region of the simulation in Figure 6 resembles the finale of the AST reception shown in Figure 2. While more accurate modeling of the near-source bathymetric interaction could be done using a propagation

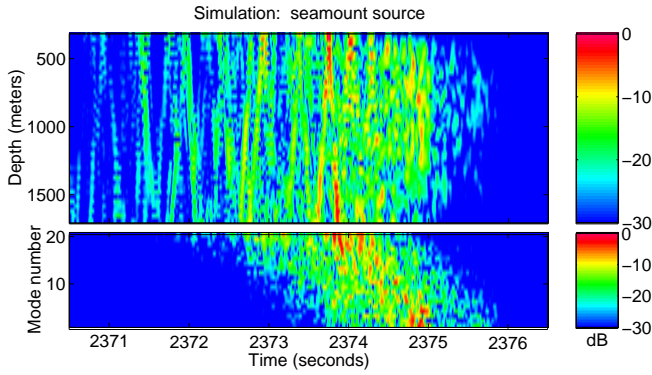


Fig. 5. Broadband PE simulation for Pioneer-Hawaii winter environment perturbed by $\frac{1}{2}$ Garrett-Munk strength internal waves. The simulation uses the measured bathymetry for the Pioneer seamount ATOC source. Top plot is the pressure time series: $20 \log_{10} |p(t)|$. Bottom plot is the associated time series for the first 20 modes.

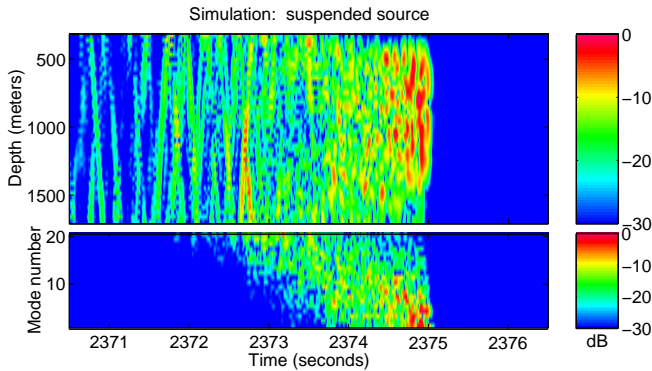


Fig. 6. Broadband PE simulation for non-sloping winter environment perturbed by $\frac{1}{2}$ Garrett-Munk strength internal waves. This simulation uses a mid-watercolumn source at the same depth as Pioneer seamount, but the seamount is not included in the bathymetry. Top plot is the pressure time series: $20 \log_{10} |p(t)|$. Bottom plot is the associated time series for the first 20 modes.

code that incorporates shear effects, these simulations provide strong evidence that the more diffuse finale region seen in the ATOC Hawaii receptions is due to bottom interaction near the Pioneer seamount source.

III. MODE PROCESSING

This paper focuses on the low-order mode arrivals in the finale region of the ATOC and AST receptions. In previous work, Worcester *et al.* described the AST experiment and gave an overview of the 28 Hz and 84 Hz receptions [12]. Dzieciuch *et al.* analyzed the finale region of the AST 28 Hz data using turning point filters [13]. Also, as noted in the introduction, Wage *et al.* examined the low-order mode arrivals at the Hawaii array for the 75 Hz ATOC source [6]. See the articles by Worcester *et al.* [14], Colosi *et al.* [15], [16], and the references therein for further discussion of related long-range propagation experiments and relevant simulation studies.

A. Short-Time Fourier Mode Processor

Figures 7 and 8 are plots of the modeshapes at the Hawaii and Kiritimati arrays, respectively. The plots show the shapes

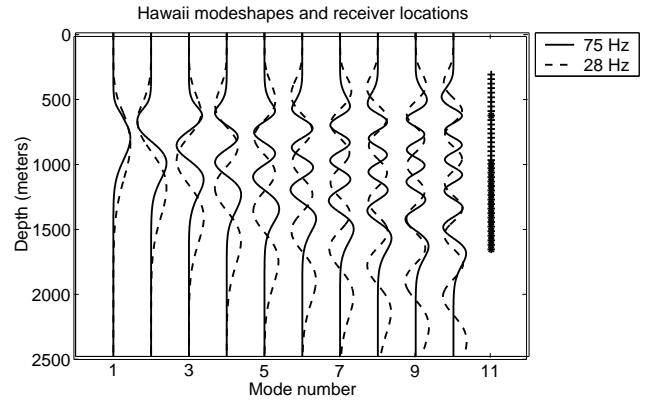


Fig. 7. Modeshapes at 75 Hz and 28 Hz for the Hawaii VLA. The hydrophone depths are shown at the far right. The '+' symbols indicate phones that remained operational throughout the experiment, and the '*' symbols indicate phones that failed prior to the AST part of the experiment.

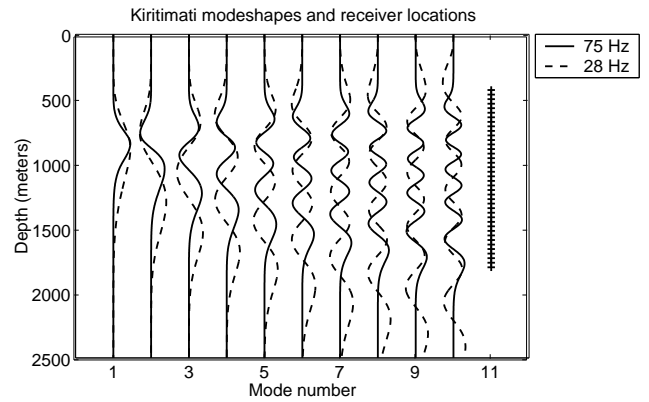


Fig. 8. Modeshapes at 75 Hz and 28 Hz for the Kiritimati VLA. The hydrophone depths are indicated by the line of '+' symbols at the far right.

at two frequencies: 75 Hz and 28 Hz. Hydrophone depths are also indicated. Each of the 40-element VLA's was designed to estimate the first 10 modes at 75 Hz.

Since the modeshapes vary with frequency, mode processing typically requires frequency decomposition to be done prior to mode filtering. In previous work [17], Wage developed a short-time Fourier processor to estimate the mode signals. The STFT processor first filters the signal into bands (where the modeshapes may be assumed constant), and then implements mode estimation for each band. Since a thorough discussion of the STFT mode processor is available in other articles [6], [18], we simply review the parameters used in the ATOC and AST processing and then present some examples.

The STFT processor designed in [6] for the ATOC Hawaii data uses a bank of bandpass filters based on a 120-point Hanning window. These filters have a bandwidth of approximately 5 Hz (± 2.5 Hz around the center frequency). Since the ATOC sample rate is 300 Hz, the 120-point Hanning window spans 0.4 seconds, meaning that the temporal resolution in the bandpass mode estimates is on the order of 0.4 seconds. The mode filter used for the ATOC Hawaii analysis is a 10-mode pseudo-inverse filter. Note that the pseudo-inverse filter for a particular mode has the advantage that it eliminates

interference from neighboring modes by placing nulls at the locations of those modes, *e.g.*, a signal propagating in mode 2 cannot leak into the mode 1 estimate. Since the ATOC array was designed to estimate 10 modes at 75 Hz, the 10-mode pseudo-inverse is well-conditioned (assuming that all 40 elements of the VLA are working). The same design parameters work for the ATOC Kiritimati receptions (the modeshapes used to compute the pseudo-inverse filter are those for the Kiritimati environment).

Processors for the AST receptions can be designed in a similar fashion. The 84 Hz receptions at Kiritimati are processed using the filterbank described above and a 10-mode pseudo-inverse mode filter. Since the array does not span the 28 Hz modes as well (see Figure 7), the pseudo-inverse is limited to 5 modes for the AST 28 Hz data at Kiritimati.

Designing mode processors for the AST receptions at Hawaii is slightly more complicated due to the hydrophone failures. The functioning top half of the VLA does not adequately sample the modes, thus the pseudo-inverse is ill-conditioned. Diagonal loading of the inverse solves the conditioning problem, at the cost of allowing energy from neighboring modes to leak into the desired mode. For the Hawaii VLA configuration, 10% diagonal loading is sufficient to stabilize the inverse. With this amount of loading, the lowest few modes at 28 Hz and 84 Hz can be estimated, with the caveat that there is more neighboring mode crosstalk than for the full array case. In the results described below, the diagonally-loaded pseudo-inverse for the 28 Hz signals includes the first five modes. For the 84 Hz AST signal, the pseudo-inverse includes 20 modes.²

B. ATOC and AST Processing Examples

In this section we examine mode estimates derived from the ATOC and AST experimental data. The discussion focuses on mode 1 since it can be estimated for all source frequencies and ranges. Recall that at 28 Hz, mode 1 has a strong arrival visible in the pressure time series at Hawaii and Kiritimati (see Figures 2 and 3).

Figure 9 shows the estimated time series for mode 1 at Hawaii for the 75 Hz ATOC source. The y-axis of the plot represents the arrival time (in seconds) within a single reception. Consecutive receptions are stacked in the x-direction. Recall from Section II that the VLA's recorded ten four-period averages for each ATOC transmission. Vertical lines in the plot separate the four-period averages within a single transmission from the four-period averages in the transmissions before and after it. Figure 9 shows the estimates for 20 transmissions, a total of 200 four-period averages, occurring over yeardays 363-366 (at the end of 1995/beginning of 1996). Nominally, there was a source transmission every 4 hours during this period, but there some of the intervals are longer due to missing or bad data. Note that the time series shown in

²The rationale for including more modes in the 84 Hz filter is that this forces more of the "aliasing" from modes not included in the estimate into the higher modes. See [6] for a discussion of the aliasing in the context of mode filtering.

Figure 9 reflect the output of the 75 Hz bin of the STFT processor for mode 1.

Figure 9 shows that there is no dominant arrival in mode 1 for a source frequency of 75 Hz. Internal wave scattering produces complicated arrival patterns containing a series of arrivals that fade in and out, sometimes disappearing over the period of a single transmission (≈ 20 minutes). Mode 1 estimates taken at 4 hour intervals show substantial differences. Based on the simulations for the seamount source, we do not expect mode 1 to have a sharp cutoff, and Figure 9 confirms that is the case. The strong arrivals are followed by 0.5-1 second of less energetic arrivals.

Figure 10 shows the mode 1 arrivals for the 84 Hz AST signal. The behavior of the 84 Hz arrivals is similar to the 75 Hz arrivals, with one notable exception: the 84 Hz data exhibit a sharp cutoff. As discussed above, this is likely due to the source being located in the middle of watercolumn rather than on a seamount.

The mode 1 arrivals at 28 Hz are a sharp contrast to the 75 Hz and 84 Hz arrivals. At 28 Hz mode 1 has one dominant arrival occurring near 2366.25 seconds. Although this arrival wanders a bit, and disappears completely for some receptions, it is far more consistent than any of the arrivals at the higher frequencies.

Figures 12, 13, and 14 show the mode 1 estimates for the 75 Hz ATOC signal, the 84 Hz AST signal, and the 28 Hz AST signal at Kiritimati, respectively. The mode 1 estimates at Kiritimati (5100 km range) are quite similar to their counterparts at Hawaii (3500 km range). In particular, the mode estimates for the AST source exhibit the sharp cutoff associated with mid-water source, whereas the ATOC cutoff is much more diffuse. The difference between the Hawaii and Kiritimati receptions is most pronounced at 28 Hz. In the Kiritimati data, mode 1 does not have a dominant arrival as it does in the Hawaii data. Instead the mode estimates for the low frequency look very similar to those for the higher frequencies. Worcester *et al.* note that the oceanography of Pioneer-Kiritimati path is much more complicated than the Pioneer-Hawaii path, particularly near the equator [12]. The more jumbled arrival pattern in mode 1 at Kiritimati is probably due to additional mode scattering caused by oceanographic features.

IV. TEMPORAL COHERENCE

Figures 9-14 demonstrate that the arrivals in mode 1 fluctuate substantially over time, *i.e.*, arrivals fade in and out over the duration of a single transmission. The purpose of this section is to quantify the temporal coherence of these arrivals, using the magnitude squared coherence (MSC) as a metric. The MSC of two random processes, x and y is defined as [19]

$$\text{MSC}(\omega) = \frac{|S_{xy}(\omega)|^2}{S_{xx}(\omega)S_{yy}(\omega)}, \quad (1)$$

where S_{xy} is the cross power spectral density and S_{xx} and S_{yy} are the auto power spectral densities. In practice, the cross power spectrum is estimated by averaging over L measurements in each frequency bin. To compute temporal

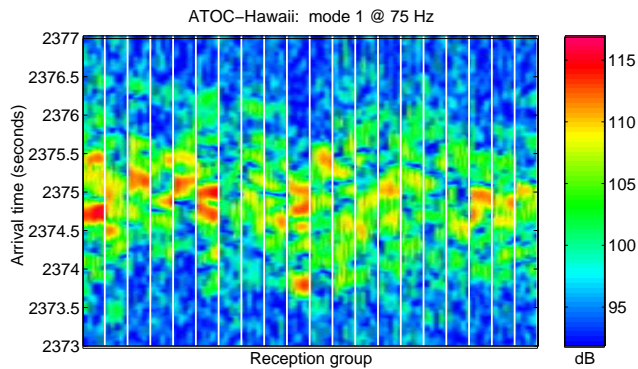


Fig. 9. Estimated mode 1 time series at Hawaii for the 75 Hz ATOC source. Arrival time is shown along the y-axis. Consecutive receptions are stacked along the x-axis. During each ATOC transmission the VLA recorded 10 four-period averages. Vertical lines separate the transmissions, which occurred at intervals of at least four hours. This plot shows receptions for yeardays 363-366 (referenced to 1995).

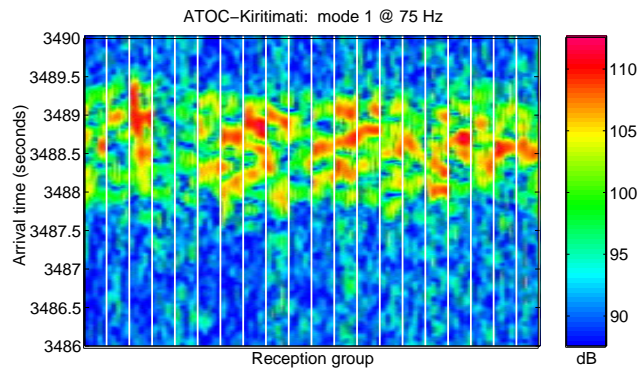


Fig. 12. Estimated mode 1 time series at Kiritimati for the 75 Hz ATOC source. Arrival time is shown along the y-axis. Consecutive receptions are stacked along the x-axis. During each ATOC transmission the VLA recorded 10 four-period averages. Vertical lines separate the transmissions, which occurred at intervals of at least four hours. This plot shows receptions for yeardays 363-366 (referenced to 1995).

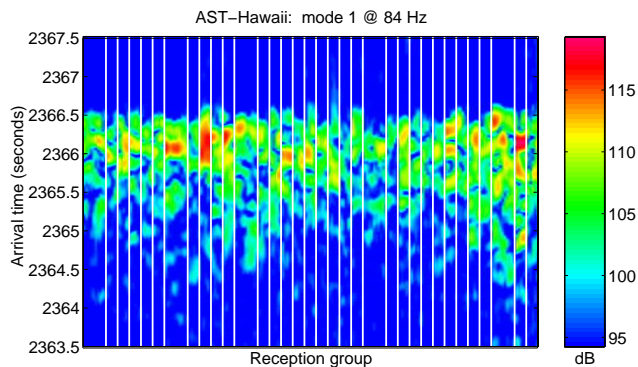


Fig. 10. Estimated mode 1 time series at Hawaii for the 84 Hz AST source. Arrival time is shown along the y-axis. Consecutive receptions are stacked along the x-axis. During each AST transmission the VLA recorded 10 or 20 four-period averages. Vertical lines separate the transmissions, which occurred at intervals of at least four hours. This plot shows receptions for yeardays 547-556 (referenced to 1995).

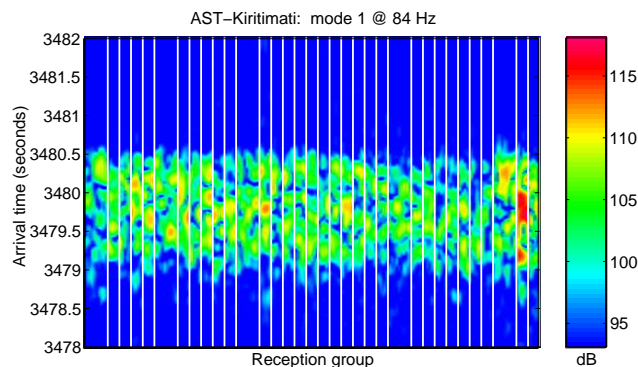


Fig. 13. Estimated mode 1 time series at Kiritimati for the 84 Hz AST source. Arrival time is shown along the y-axis. Consecutive receptions are stacked along the x-axis. During each AST transmission the VLA recorded 10 or 20 four-period averages. Vertical lines separate the transmissions, which occurred at intervals of at least four hours. This plot shows receptions for yeardays 547-556 (referenced to 1995).

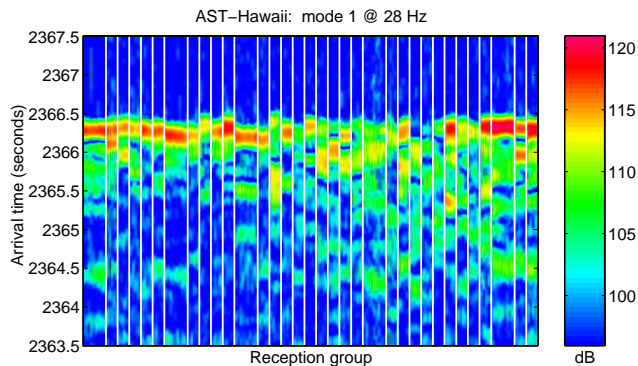


Fig. 11. Estimated mode 1 time series at Hawaii for the 28 Hz AST source. Arrival time is shown along the y-axis. Consecutive receptions are stacked along the x-axis. During each AST transmission the VLA recorded 10 or 20 four-period averages. Vertical lines separate the transmissions, which occurred at intervals of at least four hours. This plot shows receptions for yeardays 547-556 (referenced to 1995).

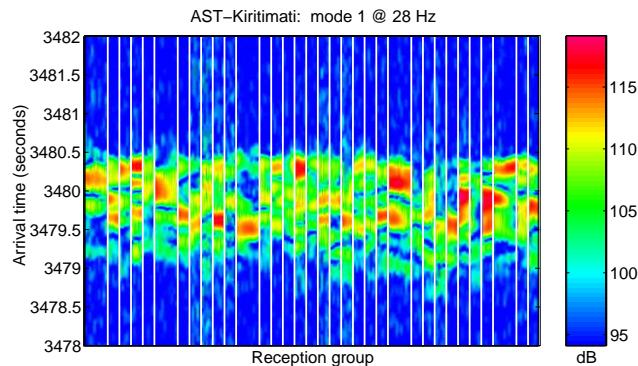


Fig. 14. Estimated mode 1 time series at Kiritimati for the 28 Hz AST source. Arrival time is shown along the y-axis. Consecutive receptions are stacked along the x-axis. During each AST transmission the VLA recorded 10 or 20 four-period averages. Vertical lines separate the transmissions, which occurred at intervals of at least four hours. This plot shows receptions for yeardays 547-556 (referenced to 1995).

TABLE I
MSC PROCESSING PARAMETERS

Data set	Receptions	Time interval	Samps/rec
Hawaii 75 Hz	20	2373.6-2375.6 s	14
Hawaii 84 Hz	34	2365.9-2366.5 s	5
Hawaii 28 Hz	34	2366.0-2366.3 s	3
Kiritimati 75 Hz	20	3487.7-3489.2 s	10
Kiritimati 84 Hz	34	3479.5-3480.5 s	7
Kiritimati 28 Hz	34	3479.6-3480.4 s	6

coherence, define the signal x as the mode estimate for the first four-period average in a reception and the signal y as the mode estimate for a four-period average recorded T minutes later. An estimate for the cross-spectrum at lag time T is

$$\widehat{S}(\omega, T) = \frac{1}{L} \sum_{l=1}^L \widehat{a}_0(\omega, l) \widehat{a}_T^*(\omega, l), \quad (2)$$

where \widehat{a}_0 and \widehat{a}_T are the estimates of the mode 1 signal for the first four-period average and the four-period average recorded T minutes later, respectively. The $*$ operator denotes the complex conjugate. Setting $T = 0$ in Equation 2 produces auto-spectrum estimates needed in Equation 1. For the ATOC and AST analysis, the series of measurements needed to estimate the auto- and cross- spectra are obtained by subsampling the output of the STFT processor. Specifically, samples are taken every 0.15 seconds, corresponding to a 62.5% overlap of the 0.4 second processing window used in the STFT.³ The sampling interval is selected to span the strongest arrivals. Table I summarizes the number of receptions, the time interval, and the resulting number of samples per reception used in the MSC computations for each of the data sets.

Figure 15 shows the estimated MSC for mode 1 at 75 Hz for the Hawaii and Kiritimati VLA's, computed using the receptions from year days 363-366. Mode 1 decorrelates rather rapidly, reaching an MSC of 0.5 at approximately 4.5 minutes. The results for the two VLA's are in good agreement, suggesting that coherence in the 75 Hz bin does not change much with range beyond 3500 km. In addition to the experimental curves, Figure 15 also shows an estimate of the MSC computed from narrowband PE simulations for the Pioneer-Hawaii path.⁴ The simulation curve is obtained by computing the mode coefficient in the 75 Hz bin for 30 realizations of the internal wave field and averaging to obtain the MSC.

Figures 16 and 17 show the MSC results for the AST receptions at 84 Hz and 28 Hz. Based on the AST measurements, mode 1 decorrelates more rapidly at 84 Hz than it does at 75 Hz. This is in contrast to the 85 Hz simulation result, which shows coherence times similar to the 75 Hz simulation. At 28 Hz, both the experimental data and the simulation show a marked increase in coherence. The simulation curve lies above both the Kiritimati and the Hawaii curves. Mode 1 at Hawaii appears less coherent than at Kiritimati. This is

³MSC processing parameters are identical to those used in the analysis of the mode arrivals in the ATOC Hawaii data set, presented in [6].

⁴A mid-watercolumn source is used.

somewhat surprising given the strong and consistent mode 1 arrivals in the Hawaii data set (see Figure 9). Additional work is planned to determine if this is an artifact of the MSC estimation method, which uses a fixed sampling interval and may miss some strong arrivals if they are not coincident with one of the predetermined sample points.

V. CONCLUSION

This paper presented a comparative analysis of the mode 1 arrivals at the Hawaii and Kiritimati arrays for the ATOC and AST experiments. Compared to the ATOC receptions, the AST receptions at both 28 Hz and 84 Hz exhibit a much sharper cutoff. Simulation results for a seamount source and a mid-watercolumn indicate that the more diffuse finale observed in the ATOC data is due to bathymetric interaction near the source. The magnitude-squared coherence was computed for mode 1 at each of the source frequencies. While the 75 Hz experimental results show good agreement with simulation, further work is needed to understand the discrepancies between the measured and simulated coherence at the other frequencies.

REFERENCES

- [1] Walter Munk and Carl Wunsch, "Ocean acoustic tomography: Rays and modes," *Reviews of Geophysics and Space Physics*, vol. 21, no. 4, pp. 777-793, May 1983.
- [2] L.B. Dozier and F.D. Tappert, "Statistics of normal mode amplitudes in a random ocean. I. Theory," *J. of the Acoustical Society of America*, vol. 63, no. 2, pp. 353-365, February 1978.
- [3] Elena Yu. Gorodetskaya, Alexander I. Malekhanov, Alexander G. Sazontov, and Nadezhda K. Vdovicheva, "Deep-Water Acoustic Coherence at Long Ranges: Theoretical Prediction and Effects on Large-Array Signal Processing," *IEEE J. of Oceanic Engineering*, vol. 24, no. 2, pp. 156-171, April 1999.
- [4] L.B. Dozier and F.D. Tappert, "Statistics of normal mode amplitudes in a random ocean. II. Computations," *J. of the Acoustical Society of America*, vol. 64, no. 2, pp. 533-547, August 1978.
- [5] John A. Colosi and Stanley M. Flatte, "Mode coupling by internal waves for multimegahertz acoustic propagation in the ocean," *J. of the Acoustical Society of America*, vol. 100, no. 6, pp. 3607-3620, December 1996.
- [6] Kathleen E. Wage, Arthur B. Baggeroer, and James C. Preisig, "Modal analysis of broadband acoustic receptions at 3515-km range in the North Pacific using short-time Fourier techniques," *J. of the Acoustical Society of America*, vol. 113, no. 2, pp. 801-817, February 2003.
- [7] The ATOC Instrumentation Group: Bruce M. Howe, Stephen G. Anderson, Arthur Baggeroer, John A. Colosi, Kevin R. Hardy, David Horwitz, Frederick W. Karig, Shaun Leach, James A. Mercer, Jr. Kurt Metzger, LeRoy O. Olson, Douglas A. Peckham, Donald A. Reddaway, Ronald R. Ryan, Ronald P. Stein, Keith von der Heydt, John D. Watson, Shirley L. Weslander, and Peter F. Worcester, "Instrumentation for the Acoustic Thermometry of Ocean Climate (ATOC) Prototype Pacific Ocean Network," in *OCEANS '95 Conference Proceedings*, San Diego, CA, October 1995, pp. 1483-1500.
- [8] Michael D. Collins, *User's Guide for RAM*, Naval Research Laboratory, Washington, D.C.
- [9] S. Levitus and T.P. Boyer, *World Ocean Atlas 1994 Volume 4: Temperature*, 1994, NOAA Atlas NESDIS 4.
- [10] S. Levitus, R. Burgett, and T.P. Boyer, *World Ocean Atlas 1994 Volume 3: Salinity*, 1994, NOAA Atlas NESDIS 3.
- [11] John A. Colosi and Michael G. Brown, "Efficient numerical simulation of stochastic internal-wave-induced sound-speed perturbation fields," *J. of the Acoustical Society of America*, vol. 103, no. 4, pp. 2232-2235, April 1998.

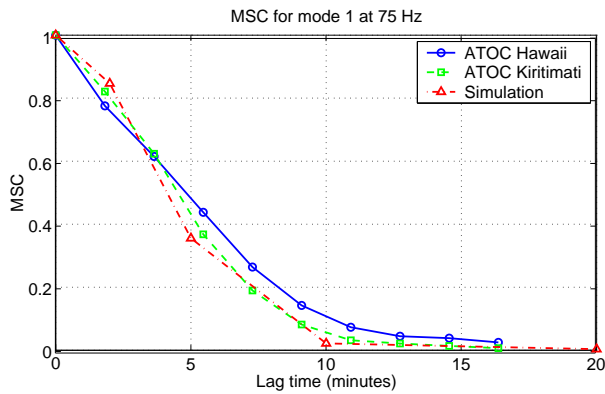


Fig. 15. Magnitude-squared coherence at 75 Hz for mode 1 as a function of the lag time between the first four-period average and successive four-period averages. The ATOC Hawaii and ATOC Kiritimati curves were derived from the receptions shown in Figures 9 and 12, respectively. The simulation result was derived from 30 narrowband PE runs.

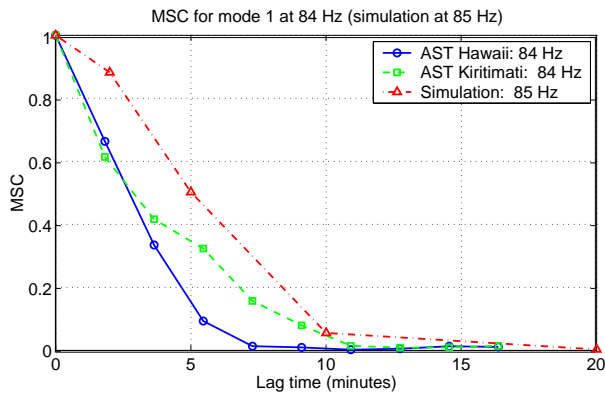


Fig. 16. Magnitude-squared coherence at 84 Hz for mode 1 as a function of the lag time between the first four-period average and successive four-period averages. The AST Hawaii and AST Kiritimati curves were derived from the receptions shown in Figures 10 and 13, respectively. The simulation result was derived from 30 narrowband PE runs. Note that the center frequency used for the simulation was 85 Hz, not 84 Hz.

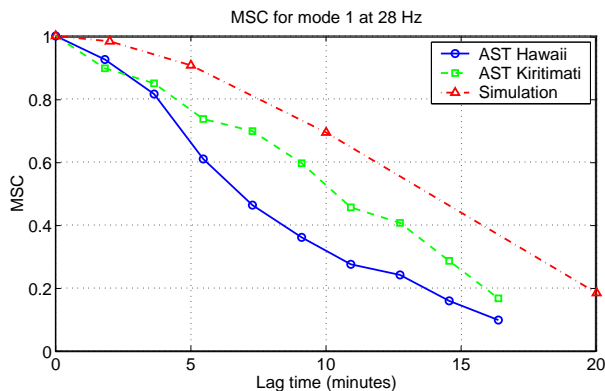


Fig. 17. Magnitude-squared coherence at 28 Hz for mode 1 as a function of the lag time between the first four-period average and successive four-period averages. The AST Hawaii and AST Kiritimati curves were derived from the receptions shown in Figures 11 and 14, respectively. The simulation result was derived from 30 narrowband PE runs.

- [12] Peter F. Worcester, Bruce M. Howe, James A. Mercer, Matthew A. Dzieciuch, and the Alternate Source Test (AST) Group, "A Comparison of Long-Range Acoustic Propagation at Ultra-Low (28 Hz) and Very-Low (84 Hz) Frequencies," in *Proceedings of the U.S.-Russia Workshop on Experimental Underwater Acoustics*, V. I. Talanov, Ed., Nizhny Novogorod, 2000, pp. 93–104, Institute of Applied Physics, Russian Academy of Science.
- [13] Matthew Dzieciuch, Peter Worcester, and Walter Munk, "Turning point filters: Analysis of sound propagation on a gyre-scale," *J. Acoust. Soc. Am.*, vol. 110, no. 1, pp. 135–149, July 2001.
- [14] Peter F. Worcester, Bruce D. Cornuelle, Matthew A. Dzieciuch, Walter H. Munk, Bruce M. Howe, James A. Mercer, Robert C. Spindel, John A. Colosi, Kurt Metzger, Theodore G. Birdsall, and Arthur B. Baggeroer, "A test of basin-scale acoustic thermometry using a large-aperture vertical array at 3250-km range in the eastern North Pacific Ocean," *J. of the Acoustical Society of America*, vol. 105, no. 6, pp. 3185–3201, June 1999.
- [15] John A. Colosi and the ATOC Group, "A Review of Recent Results on Ocean Acoustic Wave Propagation in Random Media: Basin Scales," *IEEE J. of Oceanic Engineering*, vol. 24, no. 2, pp. 138–155, April 1999.
- [16] John A. Colosi, Edward K. Scheer, Stanley M. Flatte, Bruce D. Cornuelle, Matthew A. Dzieciuch, Peter F. Worcester, Bruce M. Howe, James A. Mercer, Robert C. Spindel, Kurt Metzger, Theodore G. Birdsall, and Arthur B. Baggeroer, "Comparisons of measured and predicted acoustic fluctuations for a 3250-km propagation experiment in the eastern North Pacific Ocean," *J. of the Acoustical Society of America*, vol. 105, no. 6, pp. 3202–3218, June 1999.
- [17] Kathleen E. Wage, *Broadband Modal Coherence and Beamforming at Megameter Ranges*, Ph.D. thesis, Massachusetts Institute of Technology/Woods Hole Oceanographic Institution, February 2000.
- [18] Kathleen E. Wage, Arthur B. Baggeroer, and James C. Preisig, "Modal Analysis of Broadband Acoustic Receptions at Megameter Ranges," in *IEEE Sensor Array and Multichannel Signal Processing Workshop Proceedings*, Cambridge, MA, March 2000, pp. 102–106.
- [19] G. Clifford Carter, "Tutorial overview of coherence and time delay estimation," in *Coherence and Time Delay Estimation*, G. Clifford Carter, Ed., pp. 1–27. IEEE Press, 1993.